



ELSEVIER

Journal of Magnetism and Magnetic Materials 195 (1999) 627–638

M Journal of
M magnetism
M and
M magnetic
materials

www.elsevier.com/locate/jmmm

Magnetic and magnetomechanical properties of Ni_2MnGa

R. Tickle*, R.D. James

Department of Aerospace Engineering and Mechanics, 107 Akerman Hall, University of Minnesota, Minneapolis, MN 55455, USA

Received 2 October 1998; received in revised form 2 February 1999

Abstract

Magnetocrystalline anisotropy and magnetostrictive properties are reported for the austenitic and martensitic phases of ferromagnetic shape memory Heusler alloy Ni_2MnGa . In the low-temperature martensitic phase, the phenomenon of field-induced variant rearrangement provides a mechanism which can produce large strains, while at the same time causing anomalous effects in the apparent anisotropy. These anomalies and their effects on measured $M-H$ and torque curves are clarified. Magnetomechanical experiments were performed in the martensitic phase to characterize the work output of a suitably oriented specimen at various stresses, and with proper stress biasing of the initial microstructure produced the largest magnetostrictive strains to date of 4.3%. © 1999 Elsevier Science B.V. All rights reserved.

PACS: 75.80.+q; 75.30.Gw; 81.30.Kf

Keywords: Ferromagnetic shape memory; Giant magnetostrictive materials; Uniaxial magnetocrystalline anisotropy; Cubic-to-tetragonal transformation; Magnetomechanical properties

1. Introduction

The ferromagnetic shape memory Heusler alloy Ni_2MnGa has been the subject of recent investigation due to its unusually large magnetostriction. Experiments performed by the authors with polarized optical microscopy have confirmed that these large strains are produced by the field-induced rearrangement of martensitic variants observed in the low-temperature phase [1].

Although a great deal of previous work has detailed the characteristics of the martensitic trans-

formation in Ni_2MnGa [2–6], there is little information regarding the basic magnetic properties, i.e., anisotropy and magnetostriction constants. While determination of these properties in the high-temperature austenitic phase is straightforward, the variant microstructure produced by the martensitic transformation and the phenomenon of field-induced variant rearrangement complicate the interpretation of these properties in the low-temperature state.

In Ni_2MnGa a cubic to tetragonal transformation occurs when the material is cooled below a characteristic martensite start temperature M_s . In this transformation the cubic unit cell is contracted along one $\langle 100 \rangle$ axis and extended along the other two. Cubic symmetry permits three possible tetragonal structures called variants to form,

* Corresponding author. Tel.: +1-612-626-0593; fax: +1-612-626-1558.

E-mail address: tickle@aem.umn.edu (R. Tickle)

depending on which axis contracts. A typical martensitic microstructure consists of mixtures of the three variants in which two adjacent variants meet at one of the two possible well-defined interfaces called twin planes. While each of these variants has a unique orientation defined by its c -axis, the martensitic phase is essentially a polycrystalline state composed of variable volume fractions of the three variants.

The ferromagnetic shape memory effect refers to either the reversible field-induced austenite to martensite transformation, or the rearrangement of martensitic variants by an applied field leading to an overall change of shape. This paper concerns the latter in $\text{Ni}_{51.3}\text{Mn}_{24.0}\text{Ga}_{24.7}$. This effect has been the subject of recent investigations in alloys near the composition Ni_2MnGa [1,7,8] and in $\text{Fe}_{70}\text{Pd}_{30}$ [9]. Our experiments have demonstrated the ferromagnetic shape memory effect using the assumption that each variant has a strong uniaxial magnetic anisotropy in which the easy axis is aligned with the c -axis. Then with a properly chosen applied field direction, the field energy $-\mathbf{H}\cdot\mathbf{M}$ is reduced by volume fraction increase, through nucleation or twin boundary movement, of the variant whose easy axis is aligned with the field. One of the goals of the present research was to validate this assumption by measuring the uniaxial anisotropy of the martensite.

The results of current and previous measurements indicate that the application of fields in the martensitic state can produce any of the following processes: magnetic domain wall motion, variant nucleation, twin boundary motion, and magnetization rotation. The driving energies reflected by $\partial\mathbf{M}/\partial\mathbf{H}$ for these processes will in general be different, and all compete to reduce the applied-field energy. This has implications for the measurement of fundamental magnetomechanical properties and for the ferromagnetic shape memory effect.

In high-anisotropy materials like Ni_2MnGa , variant nucleation and rearrangement can offer lower-energy mechanisms for reducing the applied-field energy than magnetization rotation, and therefore the shape memory effect may be energetically preferred. Although these processes have no relation to magnetocrystalline anisotropy, their occurrence can significantly change the slope of

magnetization curves and therefore affect the apparent anisotropy. Anisotropy calculations based on M - H curves that do not recognize their presence will lead to erroneously small values for the true magnetocrystalline anisotropy constants. In the case of torque curves, variant rearrangement allows for the possibility of removing some or all of the microstructures responsible for generating torque in the material, which can result in field-dependent measurements where the torque actually decreases as the applied field is increased. In the case of magnetostriction measurements, variant rearrangement can produce the large strains associated with shape memory materials. Since the structural anisotropy in a tetragonal variant is large, field-inducing a change from one single variant state to another produces large strains when the short axis of the initial variant becomes the long axis of the final variant. In Ni_2MnGa , using tetragonal lattice parameter data $a = 2.95 \text{ \AA}$, $c = 2.77 \text{ \AA}$ from Zaslavskiy et al. [3], this shape change produces a maximum strain of 6.5%. In addition to the large strains caused by variant rearrangement, there is also a contribution to the magnetostriction from small distortions of the tetragonal unit cell due to the rotation of the local spontaneous moment, which we refer to as the 'ordinary magnetostriction'. Thus, the total macroscopic strain arises from both variant rearrangement and ordinary magnetostriction. Previous martensitic phase measurements of anisotropy and magnetostriction properties [10–14] have noted anomalous effects because they did not account for the shape memory effect; these are discussed in the final Section 4.

In general, any measurements in the martensitic phase of a shape memory ferromagnet are complicated by the fact that the results depend on the initial variant microstructure; this is true for both high- and low-anisotropy materials. If the initial microstructure varies due to applied fields, stresses, or repeated warming/cooling cycles, for example, then measurements for a given specimen orientation may be nonrepeatable. This fact emphasizes the importance of performing martensitic measurements on a specimen with a fixed, well-defined microstructure. By suitably biasing a specimen with stress and applied fields into a single martensitic variant, we were able to determine the uniaxial

anisotropy constant and the ordinary magnetostriction constant without the obscuring effects of variant nucleation and rearrangement; our procedure for accomplishing this is described in Section 3.2.

These fundamental property measurements are crucial for the evaluation of the ferromagnetic shape memory effect. The scheme for ferromagnetic shape memory proposed recently [1,7–9,15] is the following. The martensite is assumed to have sufficiently high magnetic anisotropy so that the magnetization stays rigidly attached to the easy axes. From the twinning orientation relationship in Ni_2MnGa it can be seen that easy axes of neighboring twin bands are nearly perpendicular to each other, so that a suitable pair of fields or a suitable arrangement of field and stress can be used to bias the material toward one variant of martensite or another, leading to a large change of shape. A micromagnetic theory [16] has been developed based on this assumption of high-martensitic anisotropy which allows arbitrary compatible microstructures of the variants of martensite to compete for the minimum of the free energy. Comparison of the predictions of this theory with measurements [1] in a wide variety of different tests clearly shows that ‘ideal’ ferromagnetic shape memory is compromised, i.e., some magnetization rotation occurs during the tests. To evaluate the propensity for magnetization rotation, and to do improved micromagnetic predictions, the basic anisotropy constant of a single variant of the martensite is needed. Our scheme for measuring this property is also relatively easy to carry out and therefore can be used as a screening tool for potential ferromagnetic shape memory materials.

In this paper we report measurements of the fundamental magnetic properties of the austenitic and martensitic phases of Ni_2MnGa , particularly those associated with the single variant martensitic state. We also report on the results of magnetomechanical tests which measure the work output and blocking stress of a suitably oriented test specimen. These tests produced the largest magnetostrictive strains to date of 4.3% and show that the present alloy can achieve large strains with an applied stress.

2. Experimental

The specimens used for all experiments described were cut using a wire EDM from a single crystal boule with composition $\text{Ni}_{51.3}\text{Mn}_{24.0}\text{Ga}_{24.7}$, as determined by a scanning electron microscope equipped with EDS, and oriented using Laue X-ray diffraction. The martensitic transformation temperature M_s was determined both visually and with DSC measurements to be $M_s \approx -10^\circ\text{C}$, with a temperature hysteresis associated with the transformation of less than 3°C . The Curie temperature T_c was determined with susceptibility measurements and found to be $T_c \approx 85^\circ\text{C}$, indicating that both austenitic and martensitic phases are ferromagnetic in this alloy. The mass of the rectangular specimen used in the work output tests was measured to give a calculated density of $\rho = 8.02 \text{ g/cm}^3$.

All $M-H$ curves and subsequent anisotropy data were obtained using a vibrating sample magnetometer. Cooling for the low-temperature anisotropy measurements was achieved using a small acrylic enclosure which fit between the pole pieces of the VSM and directed a cooled nitrogen gas stream onto the specimen.

In order to achieve a range of stable temperatures for the magnetostriction and work output measurements, a specimen stage was built which circulated cooled nitrogen gas or heated water to maintain temperatures from -20 to 70°C . The specimen stage was mounted between the pole pieces of a 1.5 T electromagnet and could be rotated for different field orientations. For the work output measurements the specimen stage incorporated a dowel pin in series with a small aluminum spring and a load cell to apply compressive stress to the specimen. The spring was designed to be soft to accommodate the large strains associated with martensitic materials without a large change in applied load. An optical microscope was mounted between the coils of the electromagnet and had free access to the top of the specimen stage. Strains for the work output measurements were determined optically using an LVDT on the microscope linear stage to measure the length of the specimen. This method became necessary after the large strains produced in the tests repeatedly debonded strain

gages on the specimen. Although nonlinearities and hysteresis in the LVDT limited the accuracy of the readings to roughly $10\ \mu\text{m}$, this amounted to only about 2% of the full-scale displacement in our specimen during the tests and so was considered acceptable.

3. Results

3.1. Austenite magnetic measurements

The high-temperature austenite measurements were performed on a thin circular disk 8.4 mm in diameter and 0.64 mm thick which was oriented with a $(1\ 1\ 0)$ normal to give $\langle 1\ 0\ 0 \rangle$, $\langle 1\ 1\ 0 \rangle$, and $\langle 1\ 1\ 1 \rangle$ directions in the plane of the disk. In order to determine the magnetic anisotropy constants

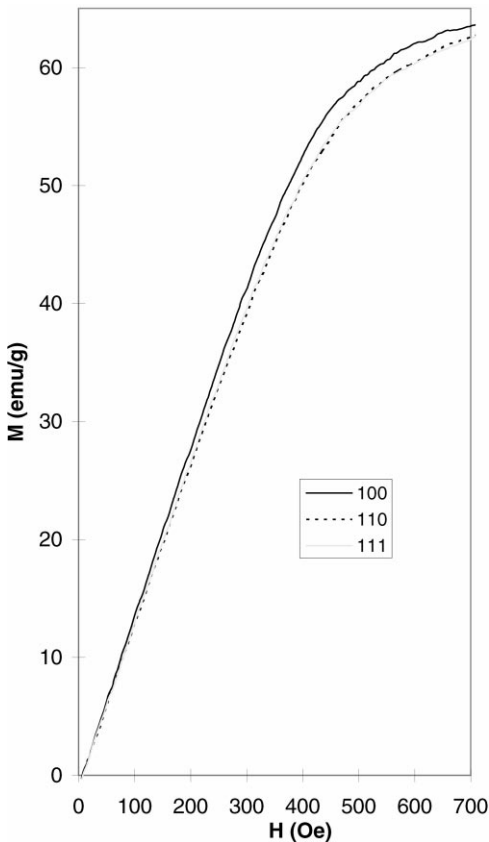


Fig. 1. M - H curve for austenite disk at -9°C .

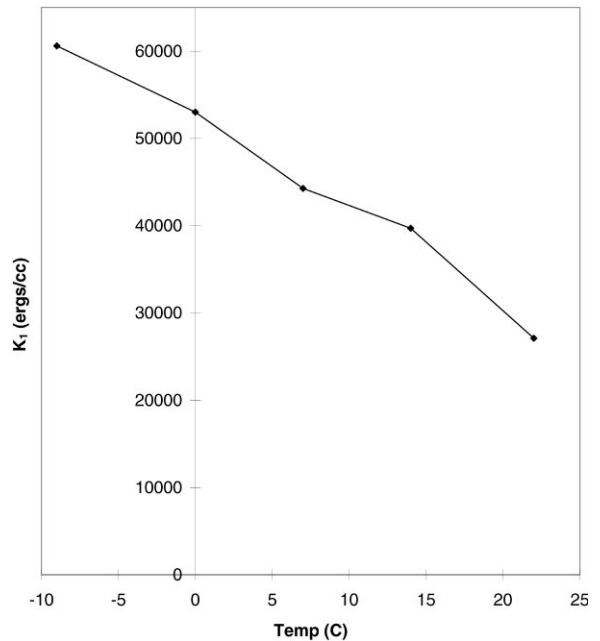


Fig. 2. Calculated K_1 values for austenite disk. Data points were obtained from areas between M - H curves at the given temperatures.

K_1 and K_2 , a series of M - H curves were performed on the austenite disk specimen at temperatures approaching the martensitic transformation temperature M_s . Fig. 1 shows the first quadrant of a typical curve performed at -9°C . Hysteresis was small for the austenitic curves at all temperatures, with $H_c \approx 5$ Oe. The data were numerically integrated to obtain values for the areas between the curves and the M -axis, and K_1 was calculated from these areas and plotted in Fig. 2. The $\langle 1\ 0\ 0 \rangle$ and $\langle 1\ 1\ 1 \rangle$ curves were essentially identical at all temperatures, implying that $K_2 = -9K_1/4$ within the resolution of the present VSM data.

The data show that the austenite clearly has $\langle 1\ 0\ 0 \rangle$ easy directions. However, the anisotropy constant K_1 is roughly an order of magnitude smaller than values typical for Fe and Ni.

The austenite magnetostriction measurements were performed on the same disk specimen with $[1\ 0\ 0]$ and $[0\ 1\ 1]$ strain gages bonded to the front and back surfaces, respectively. Magnetostriction constants $\lambda_{1\ 0\ 0}$ and $\lambda_{1\ 1\ 1}$ were determined in the

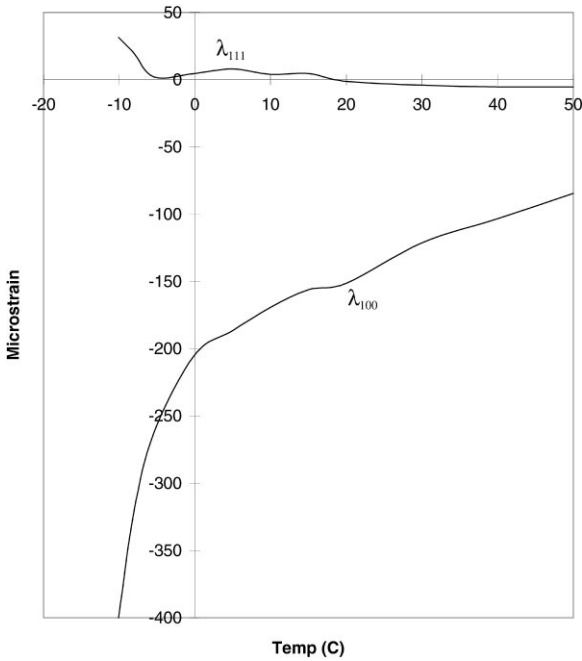


Fig. 3. Austenite magnetostriction constants λ_{100} and λ_{111} .

usual way using two separate gage readings with saturating fields in the $[100]$ ($\theta = 0^\circ$) and $[011]$ ($\theta = 90^\circ$) directions and the cubic relationships

$$\lambda_{[100] \text{ gage}} = \frac{3}{2}\lambda_{100}(\cos^2 \theta - \frac{1}{3}),$$

$$\lambda_{[011] \text{ gage}} = \frac{3}{4}\lambda_{100}(\sin^2 \theta - \frac{2}{3}) + \frac{3}{4}\lambda_{111} \sin^2 \theta.$$

Fig. 3 shows the evolution of λ_{100} and λ_{111} as transformation temperature M_s is approached on cooling. The first-order character of the martensitic transformation is signaled by the rapid change in both constants over the last 5°C above M_s .

The austenite disk specimen was also used to make a determination of the thermal expansion behavior of this alloy. Fixing the room temperature state at zero strain and subsequently warming and cooling the disk produced the results in Fig. 4. The expansion coefficient remained negative from 0°C nearly up to the Curie point. A magnetic Invar effect can be ruled out as the cause due to the fact that λ_{100} has negative sign and should produce the opposite behavior. This type of expansion anomaly indicates the presence of the pre-marten-

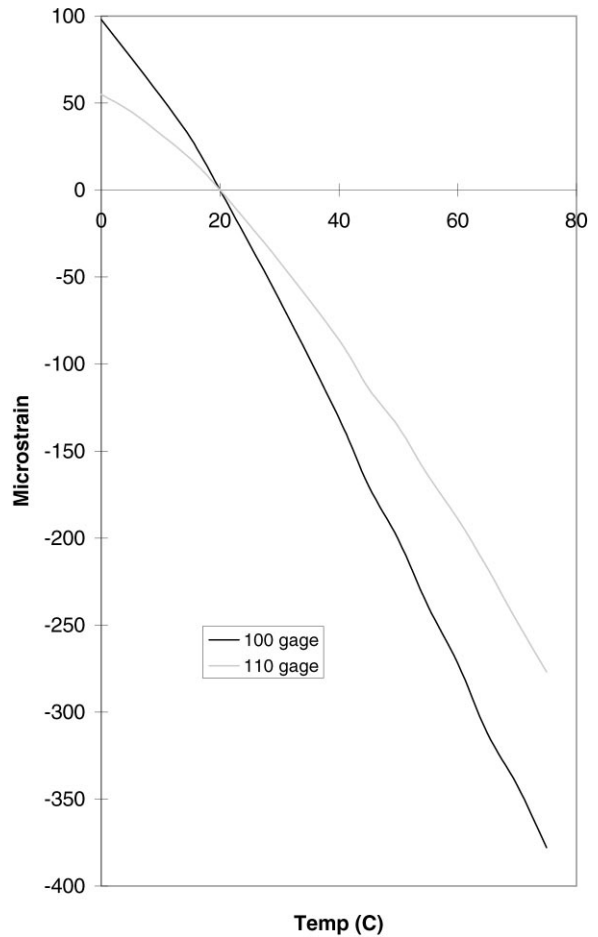


Fig. 4. Thermal strain readings from $[100]$ and $[011]$ strain gages on austenite disk while heating with no applied fields.

sitic intermediate phase confirmed previously with electron diffraction and dynamic mechanical analysis [5,6] and is consistent with the anomalous thermal data reported by Kokorin et al. [5].

3.2. Martensite magnetic measurements

The significant change in anisotropy characteristics in the martensitic phase can be appreciated by comparing typical austenite curves (Fig. 1) with Fig. 5. These curves were measured on the same disk specimen used in the austenitic measurements after cooling below M_s . They exhibit the complex characteristics associated with the ferromagnetic

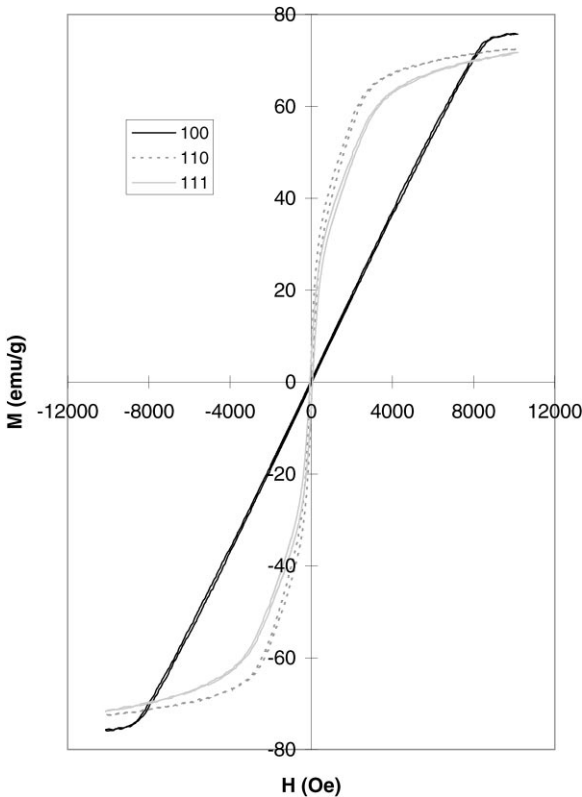


Fig. 5. M - H curve for disk specimen at -14°C after martensitic transformation. Compare with Fig. 1.

shape memory effect. Although explicit knowledge of the initial microstructure is required for a full analysis of the curves, a few characteristics are worth noting. The initial softness of the $\langle 110 \rangle$ and $\langle 111 \rangle$ curves followed by the radical change in slope at the tails indicates that magnetic domain wall motion occurred initially followed by rotation at high fields. The $\langle 100 \rangle$ curve appears to be a hard-axis curve, but comparison with the single-variant measurements of this section shows that this is not the case (see Fig. 12).

The low-temperature martensite anisotropy measurements were performed on a thin nearly square wafer $5.2\text{ mm} \times 5\text{ mm} \times 0.64\text{ mm}$ with $\langle 100 \rangle$ edges. The strategy of the tests was to compress the specimen into a single-variant state using a small fixture, shown in Fig. 6, and generate M - H curves parallel and perpendicular to the

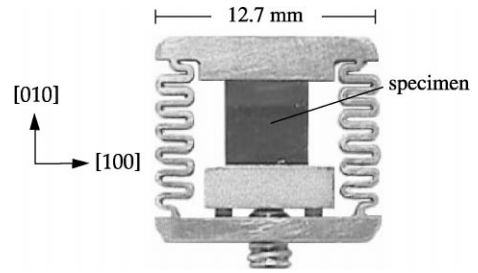


Fig. 6. Compression fixture used for martensite single-variant anisotropy measurements. Stress is applied with small set screw on fixture bottom.

compression axis. The fixture was constructed from a non-magnetic CuBe spring alloy and sized to fit in the cooling fixture used with the VSM. A small set screw allowed a fixed amount of extension to be set which applied a corresponding compressive stress to the specimen. The spring constant of the fixture was measured on a servohydraulic testing system, and for the specimen cross section used, the applied stress was $\sigma = 1.6\text{ MPa}/0.025\text{ mm}$ extension. In all tests the specimen was initially cooled with a 6000 Oe field applied along the compression axis so that both applied stress and field would favor a single-variant starting state. Since the VSM did not allow direct observation of the specimen during the measurements, initial tests of the compression fixture were performed with polarized microscopy, and confirmed that the fixture did produce a single-variant state when cooled below M_s . The specimen was sized slightly longer in the loading direction according to the measured transformation strain of the material, so that the change in shape when compressed from austenite to the single variant state created a square specimen. In this way, demagnetization effects for the two curves were kept the same, and uniaxial anisotropy constant K_u could be calculated from the area between the curves.

Three series of tests were performed with the compression fixture using extensions of 0.24, 0.28 and 0.38 mm, respectively. The amount of spring extension controlled the initial load applied to detwin the specimen, and after transformation to the single variant state also determined the final value of stress. The contraction along the compression

axis (calculated from lattice parameters and specimen geometry) produced by the transformation was 0.25 mm, so that the final stress applied for the three extensions used was 0, 1.9 and 8.3 MPa, respectively. The applied stress in the single-variant state was an important parameter in the tests, for it was required to prevent the nucleation of a second variant for applied fields perpendicular to the compression axis, and also allowed for a determination of the ordinary magnetostriction constant from stress anisotropy effects, as described below.

The results of the single-variant martensite $M-H$ curves show that the c -axis is indeed the easy axis, and the curves exhibit the expected uniaxial anisotropy. Fig. 7 shows the curves for 0 and 1.9 MPa compression. We note that the curves along the compression axis were nearly identical for all values of applied stress (see Fig. 7), as would be expected for a uniaxial material stressed along the easy axis. The effects of the applied stress can be seen when the hard-axis curves are examined. The inset graph of Fig. 7 shows a composite view of the initial portion of the hard-axis curves for both loads. With no applied load the specimen is not constrained from nucleating the second variant with easy axis perpendicular to the compression axis. This nucleation is evident in the nonlinearity of the top curve, which initially is slightly softer than the 1.9 MPa curve. As the second variant volume fraction increases, however, the specimen extends in the compression direction, and eventually becomes long enough to begin loading the spring fixture; at that point rotation begins to occur, as seen in the change in slope. The 1.9 MPa curve shows no evidence of nucleation, and the small amount of hysteresis present indicates that reversible rotation processes are occurring.

The results of the 1.9 MPa compression test were used to determine the areas between the M axis and the easy- and hard-axis curves. The uniaxial anisotropy constant calculated from this data was $K_u = 2.45 \times 10^6$ erg/cm³, roughly two orders of magnitude larger than the austenitic anisotropy constant.

The 1.9 and 8.3 MPa curves were also used to get an estimate of the magnetostriction constant for a single martensite variant. Fig. 8 shows the initial portion of the hard-axis curves for both loads. The

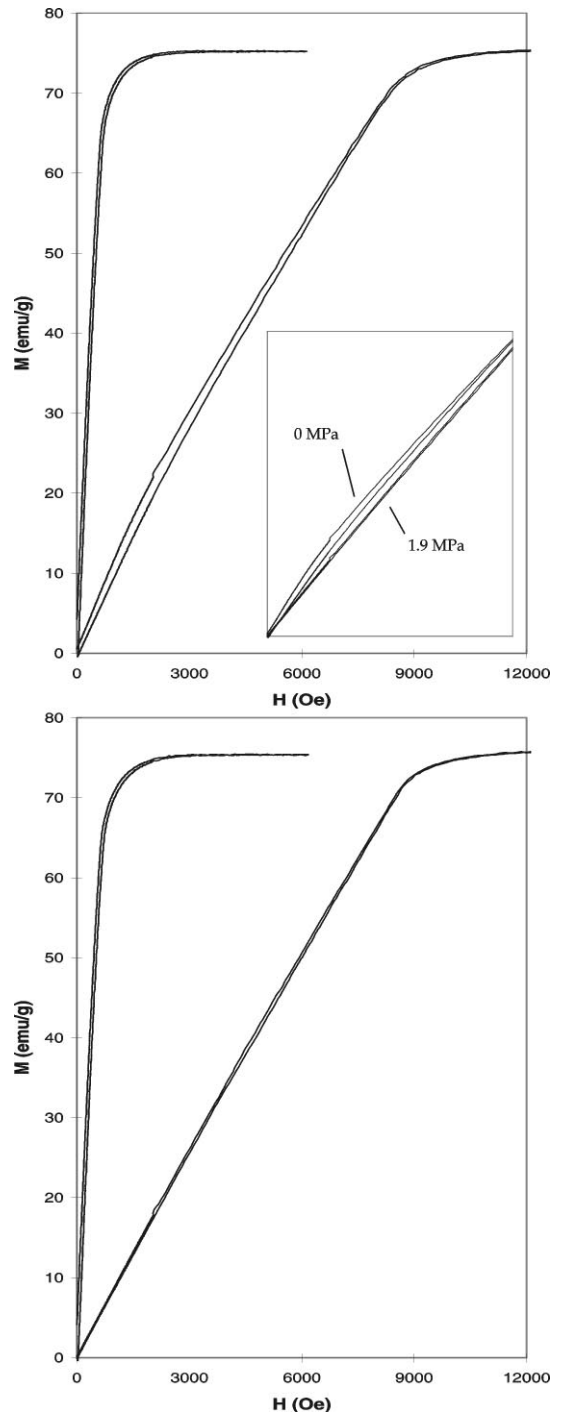


Fig. 7. Single-variant martensite $M-H$ curves at -17°C for 0 MPa (top) and 1.9 MPa (bottom) compression. Easy axis is compression axis, hard axis is perpendicular to c -axis. Inset shows initial portion of hard-axis curves for both loads.

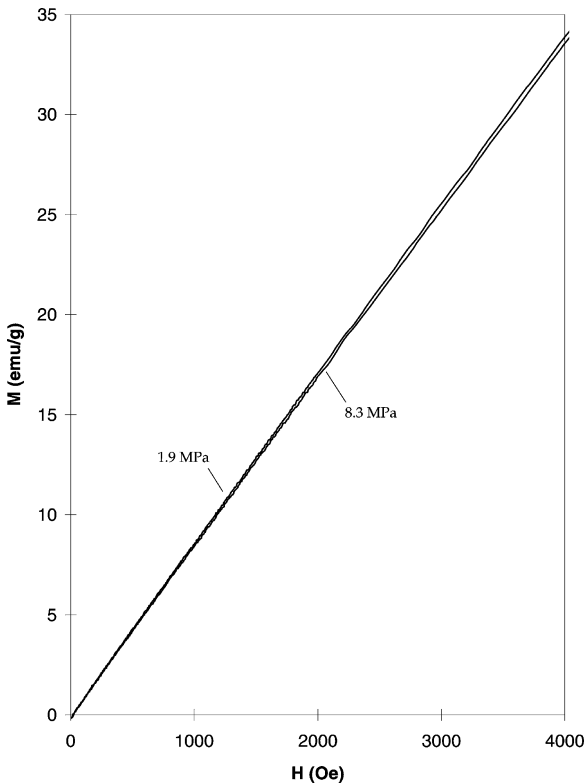


Fig. 8. Initial portion of single variant martensite M - H curves for hard axis with 1.9 MPa (top) and 8.3 MPa (bottom) compression applied to c -axis.

slopes from this data indicate that the 8.3 MPa curve saturates at slightly larger fields, implying that rotation produces an extension in the loading direction. Equating the change in magnetic energy to the change in elastic energy gives

$$\lambda_{sv} = -\frac{m_s \Delta h}{2 \Delta \sigma},$$

where Δh is the additional field required to saturate at higher stress, and $\Delta \sigma = 6.4$ MPa. Slopes for the two curves were calculated using a least-squares fit of the data and Δh was computed from these slopes at saturation. Deviation in the slopes from the linear fit gave a calculated range of $\Delta h \approx 48$ – 73 Oe, from which $\lambda_{sv} = -285 \pm 60 \mu\epsilon$.

A numerical calculation of the area between the curves provided a value of $\lambda_{sv} \approx -260 \mu\epsilon$, showing

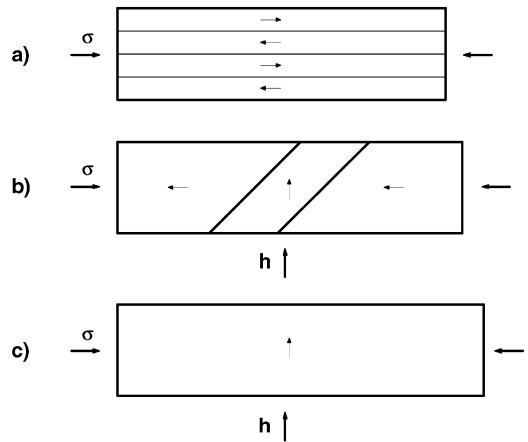


Fig. 9. Geometry of applied field and stress used in the magnetoelastic measurements. Heavy lines indicate specimen edges and twin boundaries, light lines are magnetic domain walls. The domain structures shown are based on ideal ferromagnetic shape memory. (a) Axial compression σ biases an axial single-variant state. (b) Variable transverse field is applied to introduce the transverse variant. (c) At large fields the specimen is transformed completely to the transverse variant, with large shape change and work performed against axial stress σ .

good agreement with the least-squares fit. Due to the small magnitude of ordinary magnetostriction constant λ_{sv} , stress anisotropy effects in the measurements used to obtain K_u are on the order of 10^3 erg/cm³ and therefore have been omitted.

3.3. Martensite magnetoelastic measurements

The low-temperature work output/blocking stress measurements were performed on a rectangular bar with dimensions $2 \text{ mm} \times 2 \text{ mm} \times 12.7 \text{ mm}$ and $\langle 100 \rangle$ edges. In the following discussion we refer to the long $\langle 100 \rangle$ edge of the bar as the axial direction, the short $\langle 100 \rangle$ edge as the transverse direction, and variants by their easy axes/ c -axis. A schematic view of the tests under conditions of ideal ferromagnetic shape memory is shown in Fig. 9. After cooling below M_s to -14°C , an axial compressive stress σ is applied to the specimen. This stress favors the single-variant state composed of the axial variant. Then a large transverse field (12000 Oe) is applied to introduce the transverse variant. This induces a large axial extension which does work against applied stress σ .

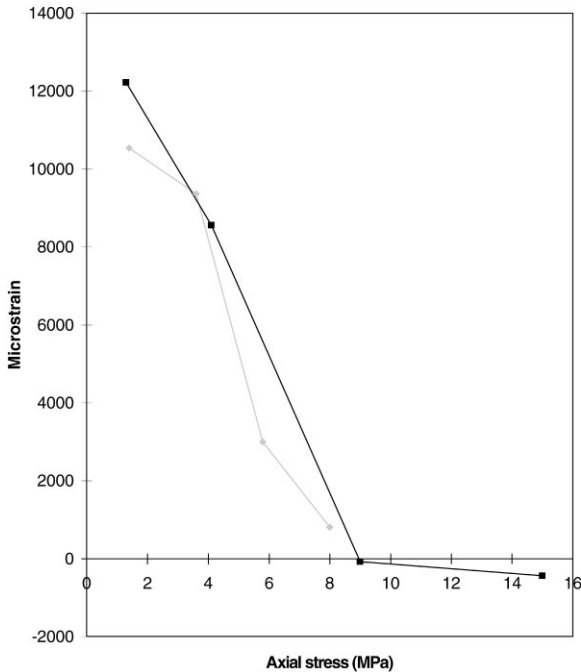


Fig. 10. Blocking stress measurements performed at -14°C . Data points represent strain induced at maximum field for fixed axial stress σ . Gray data are first series performed, black data is second series with stiffer spring.

For large enough stresses, the strain energy penalty $\sigma d\epsilon$ associated with variant rearrangement becomes too large and the field energy will be reduced by rotation processes. At this point, ignoring small strains associated with ordinary magnetostriction, the blocking stress is reached and the work output becomes zero. Two series of tests were performed with increasing values of σ to determine the blocking stress of the specimen; these are shown in Fig. 10. The data points correspond to the axial strain induced at maximum field for a fixed value of axial stress σ . In the first series, the blocking stress was not reached at 8 MPa, so the test was repeated with a slightly stiffer spring up to 15 MPa compression. The curves reflect the inaccuracy of the LVDT strain determination technique, but the trend in both indicates that the blocking stress is roughly 9 MPa.

The largest strains produced in these experiments occurred when the specimen was initially

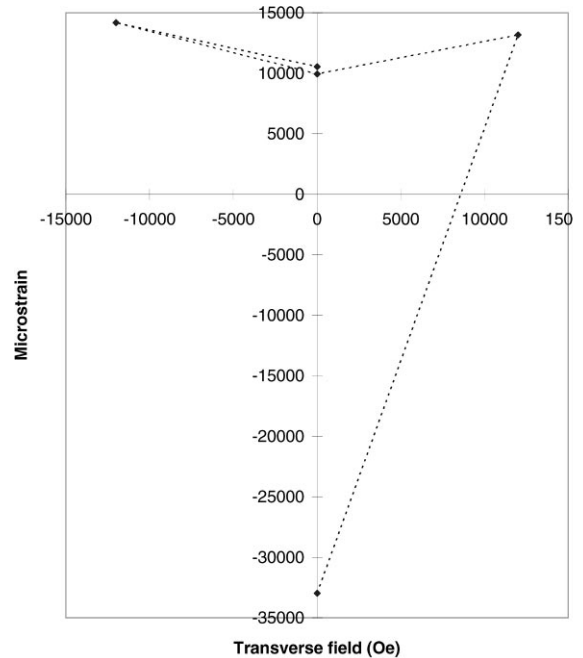


Fig. 11. Transverse field applied after biasing the initial state with 8 MPa axial compression and then removing all load. Subsequent cycling shows that stress-biased initial microstructure is required for large strains.

biased with an 8 MPa axial stress. The stress was then removed and a transverse field applied as before. When doing no work against an axial stress, the specimen was able to transform more completely at maximum transverse field, resulting in a strain of 4.3%, as shown in Fig. 11. In these data, zero strain corresponds to the undistorted austenitic state, and the dotted lines in the graph indicate that the LVDT strain determination provided no intermediate strain data, only the values of the strain at 0 and 12000 Oe transverse field. In this test the field was cycled about zero after the initial field application that produced the large strain. The results emphasize the importance that the initial microstructure has on subsequent behavior. Since there is no axial stress present to bias a single variant compressed state, the strain only decreases a small amount after the initial field is removed. This decrease can be attributed to demagnetization effects, which favor the axial variant. Subsequent

field application creates a small additional amount of axial extension, but here the starting microstructure has not been stress-biased, so the volume fraction of the axial variant is much less than in the original compressed state.

The requirement of initial microstructure bias for producing large strains directly affects the reversibility of magnetostriction measurements in ferromagnetic shape memory materials. With a proper bias stress or field applied throughout the test, the measurements are reversible; recent cycling experiments using the same specimen have produced strains of $5000\mu\epsilon$ with a constant load of 5 MPa over a period of 50–100 cycles. The amount of strain produced will be a function of the applied bias load, as in Fig. 10. Presumably smaller loads will have larger reversible components of magnetostriction; experimental confirmation of this awaits the completion of an updated setup with a capacitive based strain measurement technique with better accuracy and resolution.

4. Discussion

The experiments demonstrate that the assumption of strong uniaxial anisotropy in the martensitic variants is correct, and that the easy axis corresponds to the c -axis of the variants. Table 1 summarizes the magnetic properties of the austenitic and martensitic phases of Ni_2MnGa .

In Fig. 12 we collect the results of all martensitic M - H curves. The easy- and hard-axis curves gener-

ated in the single-variant experiments bracket the previous disk specimen curves as expected. We note that the $\langle 100 \rangle$ disk specimen curve, which has the characteristics of a hard-axis curve, is significantly

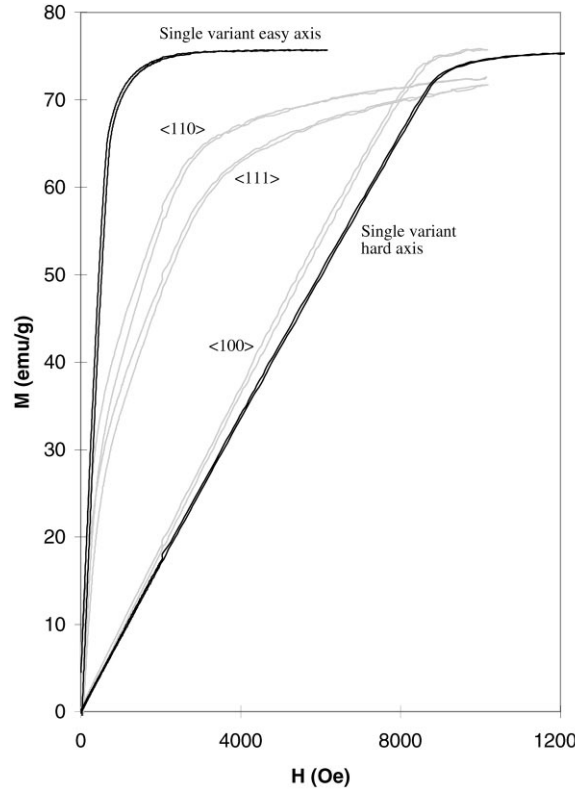


Fig. 12. M - H curves performed on single-variant specimen (black) and disk specimen (gray) in the martensitic phase.

Table 1
Summary of Ni_2MnGa magnetic properties for austenitic and martensitic phases

Temp ($^{\circ}\text{C}$)	K_1 (ergs/cm 3)	K_2 (ergs/cm 3)	λ_{100} ($\mu\epsilon$)	λ_{111} ($\mu\epsilon$)
Austenitic phase measurements				
22	2.7×10^4	-6.1×10^4	-145	-1
14	4.0×10^4	-9.0×10^4	-156	5
7	4.4×10^4	-9.9×10^4	-180	6
0	5.3×10^4	-11.9×10^4	-205	5
-9	6.1×10^4	-13.7×10^4	-360	25
Martensitic phase measurements (at -17°C)				
K_u (ergs/cm 3)			λ_{sv} ($\mu\epsilon$)	
2.45×10^6			-285 ± 60	

softer than the actual hard-axis curve. In general, $\langle 100 \rangle$ fields should energetically favor growth of one variant volume fraction over the other two, and it is likely that the $\langle 100 \rangle$ curve corresponds to the increase of the favorable variant volume fraction. The lack of softness in the curve indicates that little or no magnetic domain wall motion has occurred; we note that the presence of a large volume fraction of the favorable variant would tend to promote magnetic domain wall movement over other processes due to the small demagnetization effects of the thin sample. This suggests that the initial state contained only a small favorable variant volume fraction, and the slope of the curve indicates the larger driving energy associated with twin boundary motion.

It is worthwhile to examine previous martensitic phase anisotropy measurements in light of the present results. The measurements of Wirth et al. [11] provide a value of $K_u = 8 \times 10^5 \text{ erg/cm}^3$ for a Ni_2MnGa polycrystalline sample with an assumed isotropic distribution of variants. This weaker anisotropy can partially be explained by the mechanism of variant redistribution, which offers a lower energy pathway for reducing the applied field energy than rotation processes, thus essentially softening the hard axes, as in Fig. 12. It may also be explained by the possibility of a non-isotropic variant distribution. Matsui et al. [12] report an anomalous decrease in anisotropy with increasing field in the martensitic phase of alloy $\text{Fe}_{70}\text{Pd}_{30}$. Their measurements are based on torque curves and exhibit the torque decrease caused by variant rearrangement referred to earlier. Similar anomalous torque and magnetostriction effects were also noted in Fe_3Pt by Sasaki and Chikazumi [13], and in $\text{CeAg}_{1-x}\text{In}_x$ by Kurisu et al. [14]

In shape memory ferromagnet actuator applications, large work output at large strains requires high anisotropy to prevent the moments from simply rotating with little shape change. A simple calculation with the present data reveals that other more subtle processes may augment the anisotropy to inhibit rotation as well. Consider the two-variant state with applied stress and field shown in Fig. 9b. For large enough applied stress σ , the moments in the axial variants will rotate towards the applied field; one might expect this to occur when the

anisotropy energy plus elastic energy due to ordinary magnetostriction is less than the elastic energy incurred by variant rearrangement, i.e.

$$K_u + \sigma \lambda_{sv} < \sigma(\varepsilon_2 - \varepsilon_1),$$

where $\varepsilon_1 = -0.048$, $\varepsilon_2 = 0.013$ are the axial strains associated with the axial and transverse variants, respectively (here we consider energy per unit volume). This implies that the blocking stress occurs when

$$\sigma = \frac{K_u}{\varepsilon_2 - \varepsilon_1 - \lambda_{sv}}.$$

Using $\lambda_{sv} = -285 \mu\text{e}$ and the above transformation strains, the calculated blocking stress is $\sigma = 3.99 \text{ MPa}$, less than half of the experimentally determined value.

To understand the larger experimental blocking stress values, we consider the effects of demagnetization energy and ordinary magnetostriction at the twin boundaries in a multi-variant martensitic specimen. From the crystallography of the martensitic transformation, it can be shown [9] that the mechanical compatibility of the two variants at the twin boundary interface implies magnetic compatibility, i.e., the jump in the normal component of the magnetization is zero at the interface, and thus no poles form at these boundaries. When rotation of the magnetization in one variant occurs, however, this divergence-free condition no longer exists (e.g., consider the rotation of the axial variant magnetizations with applied transverse field in Fig. 9b). Thus magnetostatic energy due to internal divergences of the magnetization tends to inhibit rotation in certain cases. Recent work [7] indicates that it is possible to construct layered 180° magnetization sequences in the variant where rotation occurs that can reduce the magnetostatic energy at the twin boundary interface (at the expense of exchange energy). It can be shown that for any given amount of rotation, a certain volume fraction of $\pm 180^\circ$ domains exists whose average magnetization is compatible at the interface. In addition to demagnetization effects at the twin boundaries, the ordinary magnetostriction also inhibits rotation due to strain incompatibilities across the interface that arise when rotation occurs. Since these

magnetostatic and elastic mismatch energies are proportional to the number of interfaces present, it may be possible to exploit these effects through proper microstructure biasing and specimen geometry to promote even larger blocking stresses for actuator applications. Current research using magnetic force microscopy with applied fields in the martensitic phase is focused on a better understanding of the evolution of the complex domain structures in these materials.

Acknowledgements

This study was supported by ONR/DARPA N00014-95-1-1145 and -91-J-4034. It also benefited from the support of the AFOSR/MURI F49620-98-1-0433, ARO DA/DAAG55-98-1-0335, and NSF DMS-9505077.

References

- [1] R. Tickle, R.D. James, M. Wuttig, V.V. Kokorin, T. Shield, Ferromagnetic shape memory in the NiMnGa system, *IEEE Trans. Magn.*, accepted for publication.
- [2] P.J. Webster, K.R.A. Ziebeck, S.L. Town, M.S. Peak, *Phil. Mag. B* 49 (3) (1984) 295.
- [3] I.K. Zasimchuk, V.V. Kokorin, V.V. Martynov, A.V. Tkachenko, V.A. Chernenko, *Phys. Met. Metall.* 69 (6) (1990) 104.
- [4] V.V. Kokorin, V.V. Martynov, *Phys. Met. Metall.* 72 (3) (1991) 101.
- [5] V.V. Kokorin, V.A. Chernenko, E. Cesari, J. Pons, C. Segui, *J. Phys. Condens. Matter. (UK)* 8 (1996) 6457.
- [6] C. Segui, E. Cesari, J. Pons, V.A. Chernenko, V.V. Kokorin, *J. de Phys. IV* 6 (1996) C8–381.
- [7] R.D. James, R. Tickle, M. Wuttig, *Proceedings of ICOMAT-98*, 1998, accepted for publication.
- [8] K. Ulakko, J.K. Huang, C. Kantner, R.C. O'Handley, V.V. Kokorin, *Appl. Phys. Lett.* 69 (1996) 1967.
- [9] R.D. James, M. Wuttig, *Phil. Mag. A* 77 (5) (1998) 1273.
- [10] A.N. Vasil'ev, S.A. Klestov, R.Z. Levitin, V.V. Snegirev, V.V. Kokorin, V.A. Chernenko, *JETP* 82 (1996) 524.
- [11] S. Wirth, A. Leithe-Jasper, A.N. Vasil'ev, J.M.D. Coey, *J. Magn. Magn. Mater.* 167 (1997) L7.
- [12] M. Matsui, J.P. Kuang, T. Totani, K. Adachi, *J. Magn. Magn. Mater.* 54–57 (1986) 911.
- [13] T. Sasaki, S. Chikazumi, *J. Phys. Soc. Japan* 46 (6) (1979) 1732.
- [14] M. Kurisu, H. Kadomatsu, H. Fujiwara, *J. Phys. Soc. Japan* 56 (7) (1987) 2279.
- [15] R.C. O'Handley, *J. Appl. Phys.* 83 (1998) 3263.
- [16] A. DeSimone, R.D. James, A constrained theory of magnetoelasticity, preprint.